PHYSICAL REVIEW D

PARTICLES AND FIELDS

THIRD SERIES, VOLUME 37, NUMBER 11 1 JUNE 1988

Determination of α_s from energy-energy correlations in e^+e^- annihilation at 29 GeV

D. R. Wood,[α] A. Petersen,[β] G. Abrams,[α] C. E. Adolphsen,[γ] C. Akerlof,[δ] J. P. Alexander,[β] M. Alvarez,[ε,(a)] D. Amidei,[α,(b)] A. R. Baden,[α,(c)] J. Ballam,[β] B. C. Barish,[ζ] T. Barklow,[β] B. A. Barnett,[η] J. Bartelt,[β] D. Blockus,[θ] G. Bonvicini,[δ] A. Boyarski,[β] J. Boyer,[α] B. Brabson,[θ] A. Breakstone,[ι] J. M. Brom,[θ] F. Bulos,[β] P. R. Burchat,[γ] D. L. Burke,[β] F. Butler,[α] F. Calvino,[ε,(a)] R. J. Cence,[ι] J. Chapman,[δ] D. Cords,[β] D. P. Coupal,[β] H. C. DeStaebler,[β] D. E. Dorfan,[γ] J. M. Dorfan,[β] P. S. Drell,[α] G. J. Feldman,[β] E. Fernandez,[ε,(a)] R. C. Field,[β] W. T. Ford,[ε] C. Fordham,[β] R. Frey,[δ] D. Fujino,[β] K. K. Gan,[β] G. Gidal,[α] L. Gladney,[β,(d)] T. Glanzman,[β] M. S. Gold,[α] G. Goldhaber,[α] L. Golding,[α,(e)] A. Green,[β,(f)] P. Grosse-Wiesmann,[β] J. Haggerty,[α,(g)] G. Hanson,[β] R. Harr,[α] F. A. Harris,[ι] C. M. Hawkes,[ζ] K. Hayes,[β] D. Herrup,[α] C. A. Heusch,[γ] T. Himel,[β] M. Hoenk,[ζ] R. J. Hollebeek,[β,(d)] D. Hutchinson,[β] J. Hylen,[η] W. R. Innes,[β] M. Jaffre,[α] J. A. Jaros,[β] I. Juricic,[α] J. A. Kadyk,[α] D. Karlen,[β] J. Kent,[γ] S. R. Klein,[β] A. Koide,[ι,(h)] W. Koska,[δ] W. Kozanecki,[β] A. J. Lankford,[β] R. R. Larsen,[β] B. W. LeClaire,[β] M. E. Levi,[β] Z. Li,[ζ] A. M. Litke,[γ] N. S. Lockyer,[β,(d)] V. Lüth,[β] C. Matteuzzi,[β,(i)] J. A. J. Matthews,[η] D. I. Meyer,[δ] B. D. Milliken,[ζ] K. C. Moffeit,[β] L. Müller,[β,(j)] J. Nash,[β] M. E. Nelson,[ζ] D. Nitz,[δ] H. Ogren,[θ] R. A. Ong,[β] K. F. O'Shaughnessy,[β] S. I. Parker,[ι] C. Peck,[ζ] M. L. Perl,[β] M. Petradza,[δ] F. C. Porter,[ζ] P. Rankin,[β] B. Richter,[β] K. Riles,[β] P. C. Rowson,[α,(k)] D. R. Rust,[θ] H. F. W. Sadrozinski,[γ] T. Schaad,[κ,(l)] T. L. Schalk,[γ] H. Schellman,[α,(b)] W. B. Schmidke,[α] A. S. Schwarz,[γ] A. Seiden,[γ] P. D. Sheldon,[α,(m)] J. G. Smith,[ε] A. Snyder,[θ] E. Soderstrom,[ζ] D. P. Stoker,[η] R. Stroynowski,[ζ] R. Thun,[δ] G. H. Trilling,[α] R. Tschirhart,[δ] C. de la Vaissiere,[α,(n)] R. Van Kooten,[β] H. Veltman,[δ,(f)] P. Voruganti,[β] S. R. Wagner,[ε] P. Weber,[ε] A. J. Weinstein,[γ] A. J. Weir,[ζ] S. Weisz,[γ,(i)] S. L. White,[ε] E. Wicklund,[ζ] D. Y. Wu,[ζ] and J. M. Yelton[β,(o)]

[α]*Lawrence Berkeley Laboratory and Department of Physics, University of California, Berkeley, California 94720*

[β]*Stanford Linear Accelerator Center, Stanford University, Stanford, California 94305*

[γ]*University of California, Santa Cruz, California 95064*

[δ]*University of Michigan, Ann Arbor, Michigan 48109*

[ε]*University of Colorado, Boulder, Colorado 80309*

[ζ]*California Institute of Technology, Pasadena, California 91125*

[η]*Johns Hopkins University, Baltimore, Maryland 21218*

[θ]*Indiana University, Bloomington, Indiana 47405*

[ι]*University of Hawaii, Honolulu, Hawaii 96822*

[κ]*Harvard University, Cambridge, Massachusetts 02138*

(Received 5 October 1987)

We have studied the energy-energy correlation in e^+e^- annihilation into hadrons at $\sqrt{s}=29$ GeV using the Mark II detector at the SLAC storage ring PEP. We find to $O(\alpha_s^2)$ that $\alpha_s=0.158\pm0.003\pm0.008$ if hadronization is described by string fragmentation. Independent fragmentation schemes give $\alpha_s=0.10$–0.14, and give poor agreement with the data. A leading-log shower fragmentation model is found to describe the data well.

I. INTRODUCTION

The energy-energy correlation[1] (EEC) and its asymmetry (EECA) were introduced in 1978 as powerful estimators of the strong coupling constant α_s. The EEC is an energy-weighted angular correlation defined by

$$\frac{d\Sigma}{d\chi}(\chi)=\frac{1}{N}\sum_{\text{events}}^{N}\sum_{i}\sum_{j}\frac{E_iE_j}{E_{\text{c.m.}}^2}\delta(\chi-\chi_{ij})\ , \tag{1}$$

where i and j run over all particles (charged and neutral) in the event, and χ_{ij} is the angle between particles i and j. The energy-energy correlation asymmetry (EECA) is con-

ventionally defined as

$$A(\chi)=\frac{d\Sigma}{d\chi}(180°-\chi)-\frac{d\Sigma}{d\chi}(\chi)\ . \tag{2}$$

Several experiments[2-8] have studied QCD processes by examining the EEC and EECA for hadronic events in e^+e^- annihilation. Simple $q\bar{q}$ events will produce back-to-back jets which will contribute to the EEC predominantly near $\chi=0°$ and 180°. Events with hard gluon radiation, however, will populate the EEC at intermediate angles as well. In this way, the shape of the EEC is sensitive to α_s.

The advantage of the EEC over jet-counting methods is that all hadronic events are used in the measurement and no special algorithms are required to distinguish jets or clusters. The EECA has the additional advantage that many of the effects of fragmentation and experimental error contribute symmetrically to the EEC, and thus cancel in the EECA. This leads to the expectation that an α_s measurement from the EECA should be much less fragmentation dependent than other measurements. In simulations, however, even the EECA shows sensitivity to the way the gluon is imbedded in the fragmentation scheme and how energy and momentum are conserved in an event.[9-11] Nonetheless, the EECA remains a useful tool for studying hadronic events in e^+e^- annihilation.

We examine the EEC in e^+e^- collisions at a center-of-mass energy ($E_{\text{c.m.}}$) of 29 GeV. We use data from the original Mark II experiment at the SLAC storage ring PEP and from a PEP run of the Mark II after its recent upgrade. We compare our measured EEC and EECA with the predictions of second-order quantum chromodynamics (QCD) plus fragmentation models and determine α_s. We also compare our results with a leading-log shower QCD model.

In 1982, the Mark II Collaboration published a measurement of the EEC and EECA and made a first-order measurement of α_s (Ref. 12). Since that time the amount of data has increased fourfold and significant improvements have been made in QCD calculations and fragmentation models. The present results supersede the earlier ones.

II. APPARATUS

The Mark II detector has operated in several different configurations. It accumulated 211 pb^{-1} in a configuration to which we refer by its experiment number, PEP-5. This detector is described in detail elsewhere.[13] Momenta of charged particles are measured with a 16-layer cylindrical drift chamber and a high-resolution vertex drift chamber immersed in a 2.3-kG axial magnetic field. The combined information provides a momentum resolution of $(\sigma_p/p)^2=(0.025)^2+(0.011p)^2$ (p in GeV/c).

In preparation for its impending run at the SLAC Linear Collider (SLC), the Mark II was extensively upgraded. The detector was operated at PEP in the upgraded configuration, and about 30 pb^{-1} were logged. The general features of the upgrade are described in the proposal.[14] Several components of the upgrade contribute to the present analysis. A new 72-layer drift chamber[15] was installed together with a smaller trigger drift chamber.[16] This configuration, along with a new coil operating at a field of 4.5 kG, provides an improved momentum resolution for charged particles of $(\sigma_p/p)^2=(0.014)^2+(0.0026p)^2$. In addition, the acceptance for electromagnetic energy detection was increased by the addition of new end-cap calorimeters[17] which cover polar angles θ such that $0.70<|\cos\theta|<0.95$. The end caps are constructed of 36 layers of lead and proportional tubes and provide an energy resolution of $\sigma_E/E=0.2/\sqrt{E}$ (E in GeV) for photons and electrons.

The barrel calorimeter, common to both configurations, consists of eight modules of lead liquid-argon shower counters and covers a range in polar angle of about $|\cos\theta|<0.7$. Electromagnetic energy is measured in this region with a resolution of about $0.14/\sqrt{E}$.

Apart from the increased solid angle, the most important consequence of the upgrade is greatly improved two-track separation. The upgrade drift chamber, with multiple-hit readout capability and many more samples to aid in track identification, has much higher efficiency for sorting out tracks in the core of a jet.

III. TRACK AND EVENT SELECTION

All tracks are required to pass fairly tight quality and solid-angle cuts. This ensures that the momenta and angles are well measured and that the detection efficiency for these tracks is reliably described by the Monte Carlo detector simulation. The cuts used for both the PEP-5 and upgrade detectors are identical except for the solid angle and sphericity axis cuts.

We accept only those charged and neutral tracks whose polar angles at their production points satisfy $|\cos\theta|\leq 0.68$ (0.85) for PEP-5 (upgrade) data. This guarantees that only the highest efficiency region of the detector is used. For neutral particles with $|\cos\theta|\leq 0.7$, we require in addition that the detected shower be at least 3° from any of the eight cracks in ϕ between the barrel calorimeter modules.

Charged particles must have minimum transverse momenta with respect to the beam axis (p_{xy}) greater than 0.1 GeV/c. We cut on the distance of closest approach to the beam axis (r_{dca}) as follows:

$$r_{\text{dca}}\leq\begin{cases}2\text{ mm}, & p_{xy}>1\text{ GeV}/c\ ,\\ \dfrac{2\text{ mm GeV}/c}{p_{xy}}, & p_{xy}<1\text{ GeV}/c\ ,\end{cases}$$

where the momentum dependence allows for multiple scattering of low-momentum tracks. At the point of closest approach, we also require that separation from the event vertex along the beam (z) direction be less than 5 cm. Tracks with unphysically high measured momenta, $p>E_{\text{beam}}/c+3\sigma_p$, are also removed. Since no particle identification is attempted, the pion mass is assigned to all charged tracks.

Accepted neutral tracks must deposit at least 0.5 GeV in the barrel or end-cap calorimeters. In addition, each

neutral shower must be separated by at least 30 cm from any charged track of momentum greater than the observed shower energy. This requirement helps to eliminate the fake photons that arise when charged hadrons interact in the coil.

Particles satisfying the above criteria are used in the selection of hadronic e^+e^- annihilation events. Such events must have at least five charged tracks, and the energies seen in charged particles ($E_{\rm ch}$) must exceed 30% of $E_{\rm c.m.}$. Each event must have a reconstructed primary vertex consistent with the mean beam interaction point ($\Delta r < 2$ cm, $\Delta z < 10$ cm). The sphericity axis[18] is determined from the charged particles, and we require that $|\cos\theta_{\rm sph}| \leq 0.60$ (0.75) for PEP-5 (upgrade) data, where $\theta_{\rm sph}$ is the angle between the sphericity axis and the beam axis. The following cuts are made on momentum balance of charged tracks: $|\sum \mathbf{p}|/E_{\rm ch} < 0.6$ and $|\sum p_z|/E_{\rm ch} < 0.25$. These requirements help to eliminate highly boosted events such as those which arise from initial-state radiation and the two-photon production process. Since any direct photon radiation can alter the EEC, we also discard events in which hard isolated photons are detected. Such photons are defined as those with $E_{\rm shower} > 2.5$ GeV which are separated by more than 30° from all charged tracks with $p_{\rm ch} > 0.5$ GeV/c.

These event cuts are chosen to remove backgrounds from QED interactions, two-photon collisions, and beam gas collisions, and also to select well-measured events which contain ample information about the energy flow structure.

Finally, a special cut is used to remove remaining τ pairs. The charged particles are separated into two hemispheres by a plane perpendicular to the sphericity axis. For plausible τ topologies the invariant mass in each hemisphere is calculated. If this mass is less than 1.8 GeV/c^2 in both hemispheres, the event is rejected.

Only the highest quality data sets are used for this analysis. Notably, we omit PEP-5 runs in which the drift chamber was operated at reduced voltage. The samples which remain represent about 100 pb^{-1} of PEP-5 data and 24 pb^{-1} of upgrade data. The cuts select 13 823 and 5024 events, respectively. We estimate the contamination from two-photon events to be about 1%, with negligible contributions from τ pairs and beam-gas events.

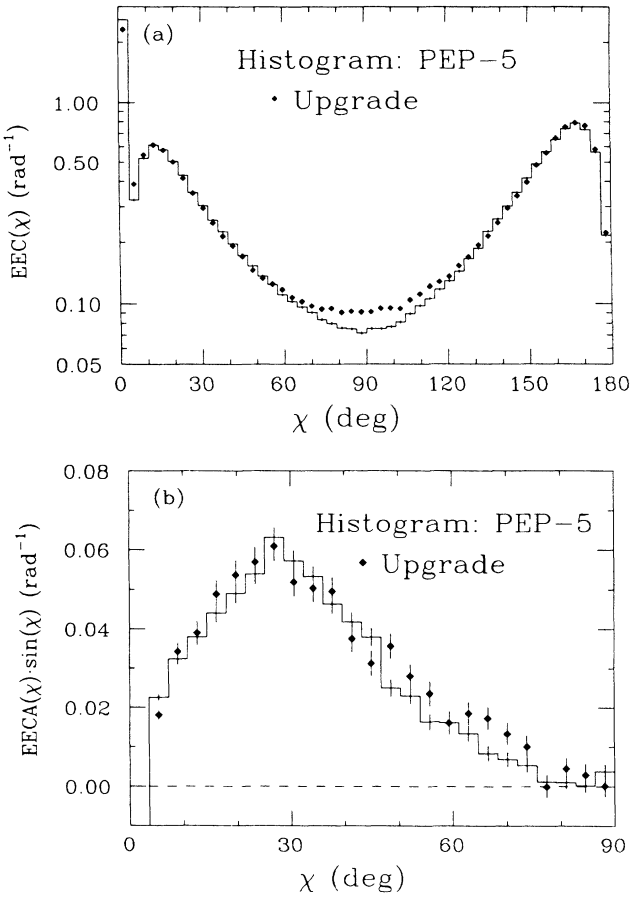

FIG. 1. (a) Raw EEC's and (b) EECA's. The data are from two detector configurations described in the text. No corrections have been made for acceptance, resolution, or efficiency.

IV. ENERGY-ENERGY CORRELATION MEASUREMENT

The EEC is accumulated from all accepted charged and neutral particles according to the formula

$$\frac{d\Sigma}{d\chi}(\chi_k)=\frac{1}{N}\sum_{\rm events}^{N}\sum_i\sum_j\frac{E_iE_j}{E_{\rm vis}^2}\left[\frac{1}{\Delta\chi}\int_{\chi_k-\Delta\chi/2}^{\chi_k+\Delta\chi/2}\delta(\chi-\chi_{ij})d\chi\right], \tag{3}$$

for 50 discrete bins in χ ($\Delta\chi=3.6°$) (Ref. 19). Note that the detected charged plus neutral energy ($E_{\rm vis}$) is used to normalize each weight rather than $E_{\rm c.m.}$ so that undetected particles have less influence on the EEC.

The uncorrected EEC and EECA distributions for both detector configurations are shown in Fig. 1. The self-correlation contribution is responsible for the spike which appears in the lowest bin in Fig. 1(a). The large peaks near 0° and 180° show the predominance of two-jet events. The width of these peaks can be attributed to both fragmentation effects and the emission of soft and collinear gluons. At intermediate angles ($30° < \chi < 150°$), however, QCD predicts that major contributions come from three- and four-parton events produced by hard-gluon radiation. The large difference between the two EEC measurements near 90° is expected from the larger solid angle coverage of the upgrade.

Before we draw conclusions from our data, we must take account of detector effects. This is accomplished by applying a simple multiplicative correction factor to the data:

$$A_{\rm cor}(\chi)=C(\chi)A_{\rm data}(\chi)\ . \tag{4}$$

The EEC itself is corrected separately in the same

manner. The correction factors C are used to compensate for the effects of initial-state radiation, detector acceptance, track- and event-selection bias, detection efficiency, and resolution.

The corrections are determined with a Monte Carlo simulation, and in principle they can depend on the parameters that go into the simulation, including the value of α_s (Ref. 20). Ideally, we would completely reevaluate the factors $C(\chi)$ for each value of α_s and each model that we consider. The computer time required is prohibitive, however, if we employ a complete detector simulation in each instance. Consequently, the correction factor C is taken to be the product C_1C_2 of two separate factors whose precise definitions will be given below, following a more detailed description of our Monte Carlo simulation. Qualitatively, the factor C_2 takes account of initial-state radiation and the gross geometry of the detector. It is sensitive to simulation-model parameters and the value of α_s. On the other hand, the factor C_1, which provides the relation between full detector simulation and the gross geometric corrections included in C_2, is close to unity and relatively insensitive to model assumptions. Thus the time-consuming calculation of C_1 need be done for only one set of model parameters, while the determination of C_2, which has to be repeated for many parameter and α_s choices, is relatively modest in its computer time requirements.

The Monte Carlo simulation is used in three modes: the event generator alone (GEN), the generator with gross geometric-acceptance corrections and initial-state radiation (AC), and a detailed full detector simulation (FS). The event generator produces a list of four-vectors for the final-state particles (including neutrinos) and is completely independent of the detector configuration. It includes the effects of QCD, fragmentation, and decays of short-lived particles. When the FS is included, the trajectory of each of the particles produced by the event generator is traced and the interactions with the active and passive material in the detector are simulated in detail. A simulated raw data image is produced which is subsequently processed by the same event reconstruction program as is used for the real data. This simulation has been extensively studied and tuned to reproduce reliably the observed detector performance.

The AC accounts for the detector effects in a simpler but more approximate manner. It uses the particle four-vectors directly from the event generator, but accepts only the detectable, stable particles $(e^{\pm},\mu^{\pm},\pi^{\pm},K^{\pm},p,\bar{p},\gamma)$ that are pointed into the acceptance region of the detector. Momenta and energies are not smeared, the detection efficiency is assumed to be 100% within the specified solid angle, and the pion mass is assigned to all charged particles. Track- and event-selection cuts, based on quantities determined from these accepted particles, are applied subsequently. The effects of initial-state radiation are included as well.[21] For many

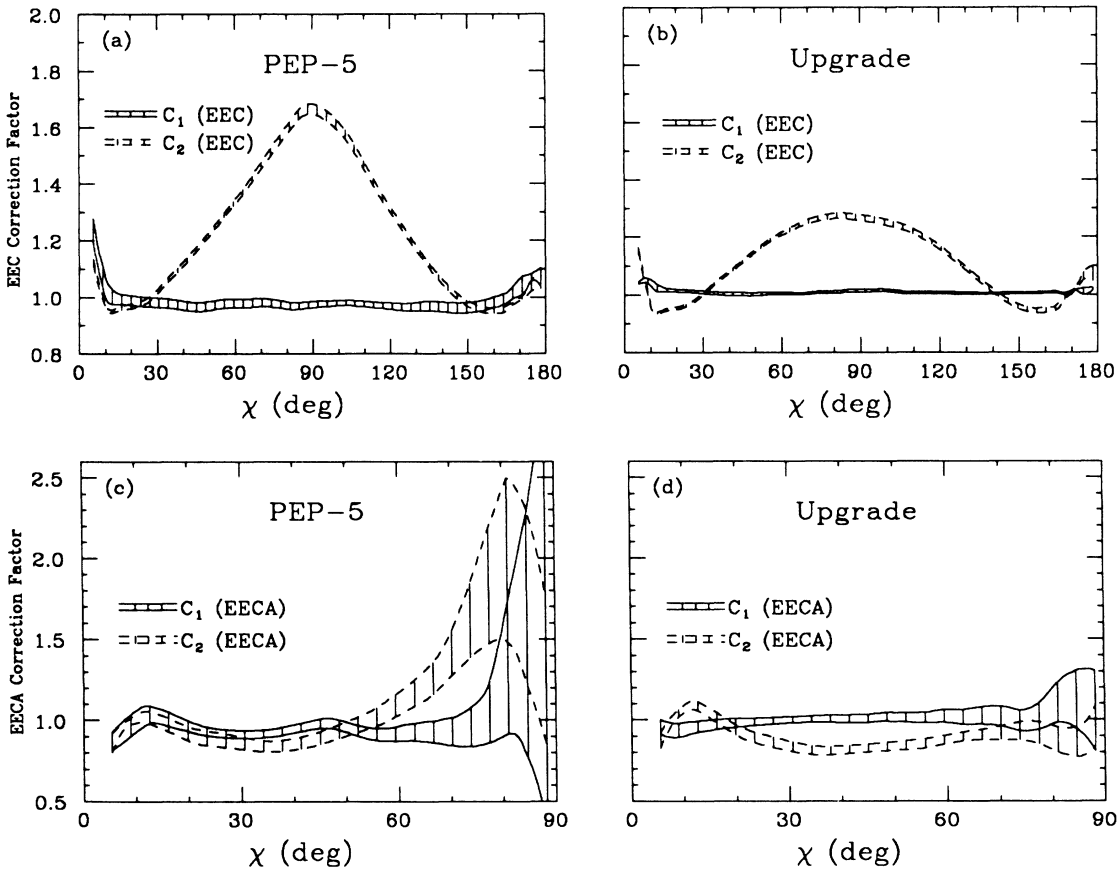

FIG. 2. Correction factors for the EEC and EECA. The two factors C_1 and C_2 (described in the text) are shown separately with solid and dashed curves, respectively. The hatched regions show the errors assigned to these factors.

studies, the AC would be grossly inadequate, but for the EEC it incorporates the most important experimental effects (solid angle, radiative corrections, and event selection bias) without requiring the time-consuming full simulation.

We define the correction factors C_1 and C_2 for the EECA as follows:

$$C_1(\chi) = A_{\rm AC}(\chi,\alpha_s^0)/A_{\rm FS}(\chi,\alpha_s^0) , \quad (5)$$

$$C_2(\chi,\alpha_s) = A_{\rm GEN}(\chi,\alpha_s)/A_{\rm AC}(\chi,\alpha_s) , \quad (6)$$

and similarly for the EEC. The correction factors C_1 are determined from large hadronic Monte Carlo samples which are carried through the full detector simulation. For these samples, there is reasonably good agreement with the data for most observables, including the EEC and EECA. Figure 2 shows the calculated C_1 and C_2 for the two detector configurations. Bands are used to indicate the systematic uncertainties on these factors. The bin to bin fluctuations are smoothed out in the central region of the EEC corrections ($14.4° \le \chi \le 165.6°$) by convolution with a Gaussian. For the asymmetry correction, Gaussian smoothing is used for $\chi \ge 10.8°$. The large corrections to the EECA near 90° are of little consequence because the asymmetry itself is vanishing in this region. Note that, aside from this, the corrections made with C_1 are $\lesssim 10\%$ within the regions used for α_s studies.

In order to estimate the systematic errors on C_1, we separate the Monte Carlo events into three subsamples according to the number of charged particles generated: low multiplicity ($n_{\rm ch} \le 10$), medium multiplicity ($n_{\rm ch} = 12, 14$), and high multiplicity ($n_{\rm ch} \ge 16$). The combined sample approximately reproduces the measured average multiplicity of 12.9 ± 0.6 (Ref. 22), and this decomposition divides the sample into roughly equal thirds. The quantity C_1 is calculated separately for the high- and low-multiplicity subsamples, and the deviation between the two is used as an estimate of the systematic error. This should be considered a realistic estimate of the systematic error because the largest contribution to deviations from unity in C_1 is the loss of detected tracks in crowded environments. The contributions to the systematic error from Monte Carlo statistics are also included where they are appreciable. The widths of the bands in Fig. 2 indicate the sizes of the total systematic errors.

In addition, C_1 is checked for model dependence. Figure 3 shows a comparison between two determinations of C_1 for the PEP-5 detector. One is obtained from a sample of Lund string[23] Monte Carlo events and is shown with the errors discussed above. The other is determined from a comparable independent-fragmentation[24] Monte Carlo sample. The two calculations of C_1 are consistent within errors. Similar checks for the upgrade detector give very good agreement between calculations of C_1 with string fragmentation and shower models.

For the PEP-5 detector, the tracking efficiency has been studied in detail. In hadronic events, the Monte Carlo sample has been found to overestimate the true single-track efficiency by $1.5\% \pm 3.0\%$ (Ref. 25). The effects of overestimating the efficiency are evaluated by analyzing a large block of data (not used elsewhere in our analysis) for which the drift chamber was operated at reduced voltage, resulting in a 10% degradation in efficiency. From a comparison between this and the higher-quality data, we conclude that the efficiency uncertainties can be neglected in the EEC and EECA measurements.

For the upgrade data, we study the effect of the two-track separation on the efficiency. The two-hit resolution is altered in the detector Monte Carlo simulation to be slightly worse than what is observed in the data, and this is found to have a negligible effect on C_1.

We make an explicit check for any bias remaining from a dependence of C_1 upon α_s. We calculate C_1 for Monte Carlo samples in which the two-, three-, and four-parton components are reweighted to simulate values of α_s from 0.11 to 0.20. C_1 (EECA) changes by less than 1% for $\chi > 30°$ over this entire range of α_s for both PEP-5 and upgrade configurations.

For the purpose of determining the best detector-independent measures of the EEC and EECA, the corrections C_2 are calculated from a large AC Monte Carlo

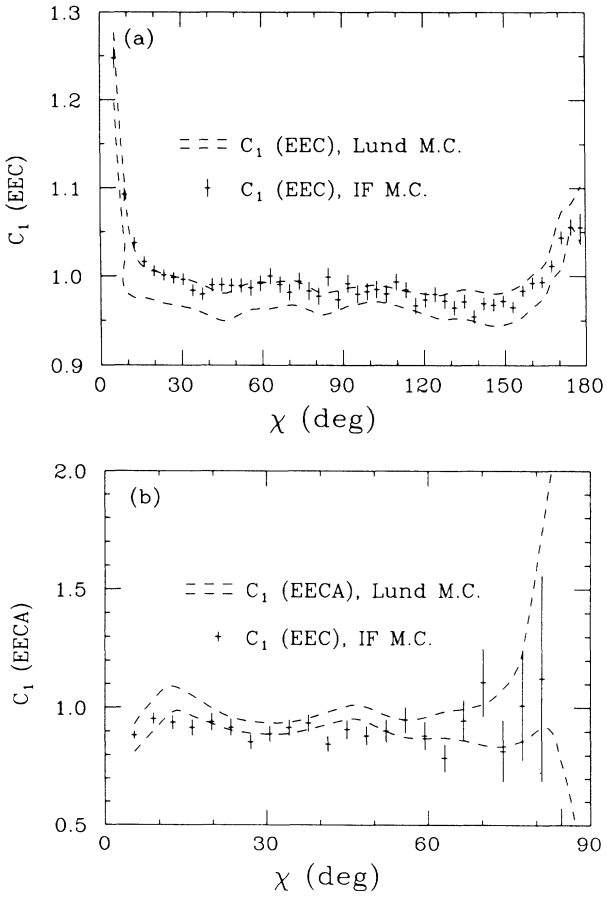

FIG. 3. Comparison of PEP-5 C_1 from Lund and IF samples. The dashed band shows C_1 as determined from the Lund sample. The width of the band indicates the size of the systematic errors assigned to C_1. The points show C_1 from the independent fragmentation sample, and the error bars are from the IF Monte Carlo statistics.

sample generated with a value of $\alpha_s=0.158$ with the Lund string Monte Carlo[23] simulation and the Gottschalk and Shatz matrix element.[26] This value of α_s corresponds to our measurements described in Sec. V. To establish the errors on C_2 due to α_s uncertainty and model dependence, we recalculate C_2 with four different Monte Carlo samples: Lund string with $\alpha_s=0.141$, Lund string with $\alpha_s=0.173$, Hoyer independent fragmentation[27] with $\alpha_s=0.105$, and Lund shower[23] with $\Lambda_{\rm LLA}=400$ MeV. The two string Monte Carlo samples represent roughly the 2σ limits (statistical and systematic) of our measured value of α_s. The comparison of the four calculations yields an estimated uncertainty in C_2 for each bin in χ, and this is used to assign the systematic errors which appear in Fig. 2.

Our fully corrected EEC and EECA distributions with separate statistical and systematic errors are given in Tables I and II. Note that when summing bins in χ, the statistical errors may be added in quadrature, but the systematic errors are strongly correlated. To allow simple comparisons with models[28] and other experiments, we give here the integrals over the conventional intervals:[29]

$$\int_{57.6^\circ}^{122.4^\circ}\frac{d\Sigma}{d\chi}(\chi)d\chi=\begin{cases}0.1486\pm0.0005\pm0.0018\pm0.0014, & \text{PEP-5},\\ 0.1458\pm0.0007\pm0.0006\pm0.0010, & \text{upgrade},\end{cases}$$

$$\int_{28.8^\circ}^{90^\circ}A(\chi)d\chi=\begin{cases}0.0297\pm0.0008\pm0.0010\pm0.0016, & \text{PEP-5},\\ 0.0306\pm0.0010\pm0.0006\pm0.0010, & \text{upgrade},\end{cases}$$

where the first error is statistical and the second and third are the systematic errors which result from the uncertainties on C_1 and C_2, respectively.

The fully corrected data are shown with combined errors in Fig. 4. The agreement between the two detector configurations is quite good. In Fig. 5 we compare our EEC and EECA directly to those of MAC (Ref. 6), which were obtained at the same energy.

V. α_s DETERMINATION

To measure α_s, we compare our data with the $O(\alpha_s^2)$ perturbative QCD predictions for $e^+e^-\rightarrow$quarks and gluons. We use the recent dressed matrix element calculation of Gottschalk and Shatz.[26] Previous measurements used either the ERT (Ref. 30) or FKSS/GKS (Ref. 31) matrix element calculations. The differences among these are discussed in detail in Ref. 26, and the new calculation incorporates significant terms that are neglected in the GKS matrix element. The calculation assumes massless partons, and quark masses are inserted *a posteriori*. The individual two-, three-, and four-parton cross sections are separated by employing a $y_{\rm min}$ cutoff of 0.015, where $y_{ij}=(p_i+p_j)^2/s$ is the scaled invariant mass of a pair of partons. We verify that the predicted EECA is stable at

TABLE I. Fully corrected EEC, in units of 10^{-3} rad^{-1}.

χ (deg)	PEP-5 EEC	Upgrade EEC	χ (deg)	PEP-5 EEC	Upgrade EEC
0.0–3.6	1633±9±103	1645±15±37	90.0–93.6	122±2±2	117±3±1
3.6–7.2	451±6±15	468±8±3	93.6–97.2	121±2±2	121±3±1
7.2–10.8	563±6±20	576±8±7	97.2–100.8	122±2±2	121±3±1
10.8–14.4	583±5±16	589±7±7	100.8–104.4	125±2±2	119±2±1
14.4–18.0	556±5±11	557±7±4	104.4–108.0	133±2±2	130±3±1
18.0–21.6	486±4±9	489±6±3	108.0–111.6	140±2±2	137±3±1
21.6–25.2	415±4±8	405±5±3	111.6–115.2	144±2±2	147±3±1
25.2–28.8	345±3±6	347±5±2	115.2–118.8	154±2±2	152±3±1
28.8–32.4	306±3±6	299±4±2	118.8–122.4	163±2±2	159±3±1
32.4–36.0	268±3±5	260±4±2	122.4–126.0	174±2±3	175±3±1
36.0–39.6	241±3±4	228±3±2	126.0–129.6	192±2±3	188±3±1
39.6–43.2	215±2±4	209±3±1	129.6–133.2	208±2±4	210±4±1
43.2–46.8	194±2±3	190±3±1	133.2–136.8	243±3±5	226±4±2
46.8–50.4	178±2±3	167±3±1	136.8–140.4	268±3±5	256±4±2
50.4–54.0	165±2±3	156±3±1	140.4–144.0	300±3±6	296±5±2
54.0–57.6	156±2±3	149±3±1	144.0–147.6	340±4±7	333±5±3
57.6–61.2	144±2±2	142±3±1	147.6–151.2	393±4±8	384±6±3
61.2–64.8	137±2±2	132±3±1	151.2–154.8	457±4±10	463±7±4
64.8–68.4	134±2±2	128±2±1	154.8–158.4	526±5±11	531±7±5
68.4–72.0	130±2±2	123±2±1	158.4–162.0	611±5±13	633±8±6
72.0–75.6	124±2±2	119±2±1	162.0–165.6	700±6±15	723±9±7
75.6–79.2	121±2±2	121±3±1	165.6–169.2	781±7±16	783±11±4
79.2–82.8	118±2±2	116±2±1	169.2–172.8	760±8±24	790±12±5
82.8–86.4	119±2±2	118±2±1	172.8–176.4	627±8±14	626±11±10
86.4–90.0	116±2±2	117±2±1	176.4–180.0	243±5±9	243±7±6

TABLE II. Fully corrected EECA, in units of 10^{-3} rad^{-1}.

χ (deg)	PEP-5 EECA	Upgrade EECA
0.0–3.6	−1389±9±97	−1399±15±31
3.6–7.2	180±6±17	161±10±11
7.2–10.8	199±9±14	214±13±11
10.8–14.4	183±10±12	186±14±8
14.4–18.0	154±8±9	173±12±7
18.0–21.6	128±6±7	146±10±6
21.6–25.2	112±5±6	126±8±5
25.2–28.8	112±5±6	115±7±5
28.8–32.4	88±4±4	85±6±3
32.4–36.0	73±3±3	73±5±3
36.0–39.6	59±3±3	66±5±3
39.6–43.2	52±3±3	47±4±2
43.2–46.8	47±3±2	37±4±1
46.8–50.4	30±3±2	40±4±2
50.4–54.0	26±2±2	30±3±1
54.0–57.6	18±2±1	25±3±1
57.6–61.2	19±2±1	17±3±1
61.2–64.8	16±2±1	19±3±1
64.8–68.4	11±2±1	18±3±1
68.4–72.0	10±3±1	13±3±1
72.0–75.6	9±3±2	10±3±1
75.6–79.2	2±3±1	0±3±0
79.2–82.8	3±4±1	5±3±1
82.8–86.4	1±5±0	3±3±1
86.4–90.0	9±4±8	0±3±0

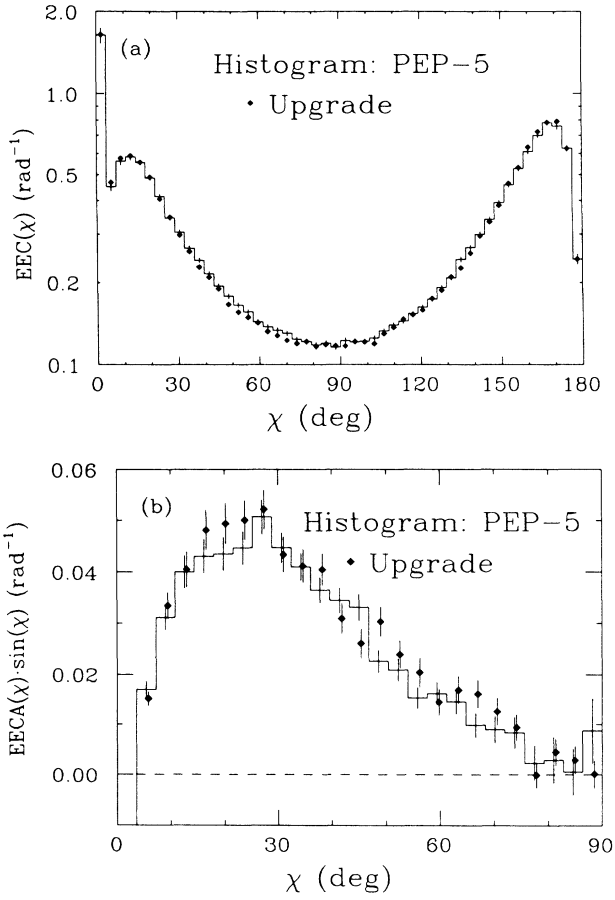

FIG. 4. Fully corrected data. The fully corrected EEC and EECA are shown separately for the PEP-5 and upgrade detectors. The errors shown are the sum in quadrature of the statistical and systematic errors.

small values of this infrared cutoff, as shown in Fig. 6.

To account for fragmentation effects, we use the Lund string model with the Lund symmetric fragmentation function. This model is quite successful in describing the general features of our data,[28] and, in particular, it favorably reproduces the distribution of particles in three-jet events.[32,33] We comment on the effects of fragmentation models more fully in Sec. VI. The parameters of the model have been initially chosen to describe the global features of our data, including distributions of multiplicity, momentum, and sphericity.[28,34]

To determine α_s, we compare our data with high-statistics samples of Monte Carlo events generated with five different values of α_s. Only the detailed detector corrections represented by the factor $C_1(\chi)$ are applied to the data, and the radiative and gross acceptance effects are included in the Monte Carlo simulations to which the data are compared. Thus the effects of α_s on the properties of the generated events and the geometric acceptance are properly included.

Our best estimates of α_s are obtained from a χ^2 comparison between the data and Monte Carlo EECA distributions as just described. We limit the sensitivity to fragmentation effects in $q\bar{q}$ events by utilizing the EECA information only for a limited region in χ, namely $\chi \geq 28.8°$ (17 bins). Only statistical errors are considered in the χ^2 calculations. The results are shown in Fig. 7. Parabolas are fitted to the χ^2 points, and from the positions of the minima and the curvatures we obtain the values and errors of α_s:

$$\alpha_s = \begin{cases} 0.155 \pm 0.004, & \text{PEP-5,} \\ 0.159 \pm 0.004, & \text{upgrade,} \end{cases}$$

where the errors are statistical only. These values each correspond to $\chi^2 \approx 20$ for 16 degrees of freedom.

The statistical error on the upgrade measurement is comparable to that from the PEP-5 measurement in spite of the smaller number of events. This is a consequence of the larger solid angle and higher efficiency of the upgrade detector, since the statistical precision of the EECA measurement improves not only with the number of events but also with the number of particles detected in each event.

The details of the fragmentation introduce additional systematic uncertainties into the α_s determination. Hadronization in the string model is governed largely by the parameters σ_q, A, and B. The momenta of hadrons along the string direction are obtained from the symmetric Lund fragmentation function[35]

$$f(z) = \frac{1}{z}(1-z)^A \exp(-Bm_\perp^2/z) , \tag{7}$$

where $m_\perp^2 = (m^2 + p_\perp^2)$ and z is the fraction of $(E + p_\parallel)$ ac-

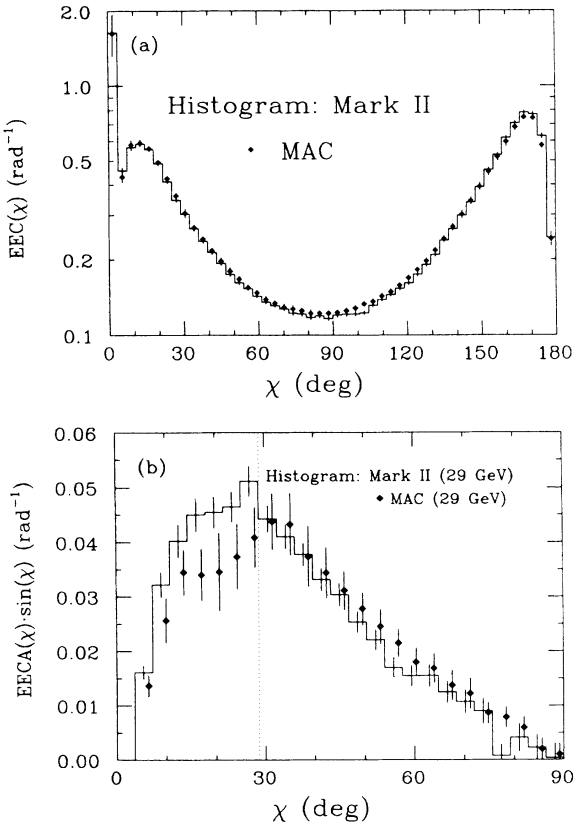

FIG. 5. Comparison to MAC experiment. The fully corrected EEC and EECA (PEP-5 and upgrade combined) are compared with fully corrected data from the MAC experiment. The MAC EECA points are offset by 1° for clarity. The region of the EECA above the dotted line in (b) is used to measure α_s.

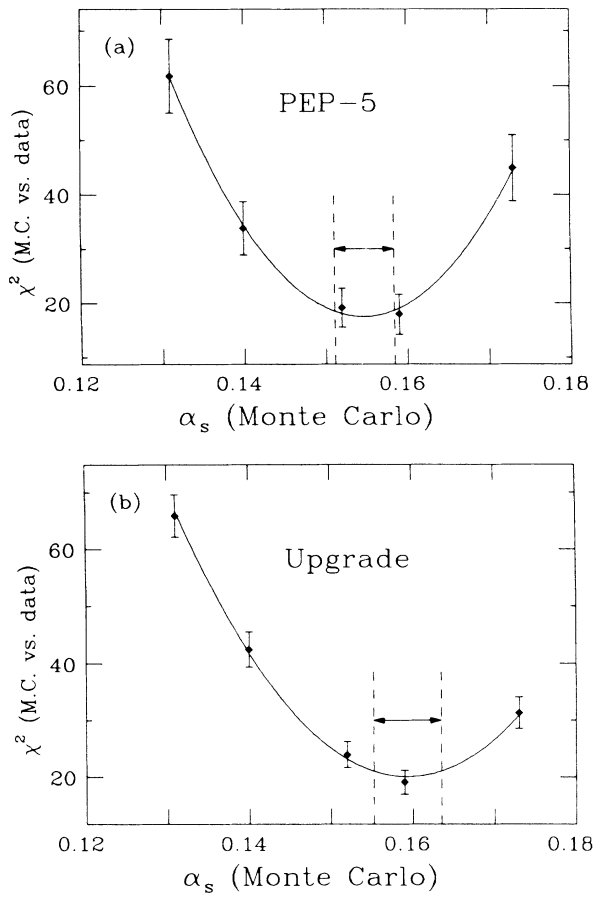

FIG. 7. χ^2 comparison between data and Monte Carlo simulations. The points represent a χ^2 (for 17 data points) calculated from comparing the EECA with Monte Carlo data generated at several values of α_s. The errors represent the expected variation of this quantity with the Monte Carlo statistics. The curves are parabolas fitted through the points, and the locations of the minima indicate the best values of α_s. The vertical lines show the 1σ statistical errors on α_s.

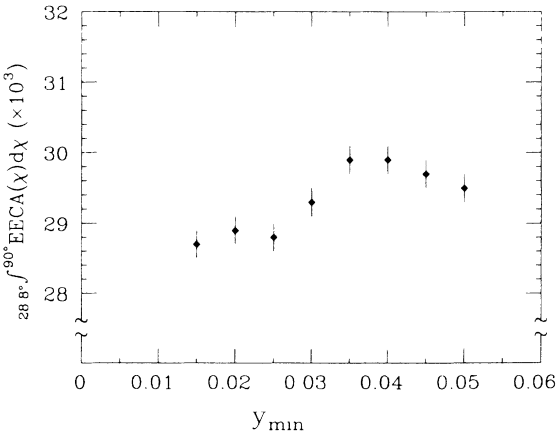

FIG. 6. Cutoff stability of the EECA. The integrated asymmetry is shown from Monte Carlo samples generated with the Gottschalk and Shatz matrix element and Lund string fragmentation for several values of the infrared cutoff parameter $y_{\min}$.

quired by the hadron. The transverse momenta of quarks are distributed according to a Gaussian of width σ_q. The fragmentation parameters A and B are strongly correlated, and therefore B is left fixed at 0.7 GeV^{-2} while A is varied over a range that agrees with the observed charged-particle multiplicity, namely, $0.6 \leq A \leq 1.2$. A small correlation exists between the multiplicity and the input value of α_s which is accounted for in the systematic errors. If both A and B are varied so as to maintain a constant multiplicity, the variations in the EEC are negligible. The range of σ_q is confined to be between 0.240 and 0.290 GeV in order to give reasonable agreement with the distribution of particle momenta normal to the sphericity plane ($p_\perp^{\text{out}}$) (Ref. 28). The detailed shape of the EECA for $\chi > 30°$ is insensitive to small changes in these parameters, and therefore the integrated EECA is used to investigate the systematic errors. Figure 8 shows the changes introduced by varying A and σ_q.

We have also tried using Peterson[36] fragmentation functions for heavy quarks. The measured spectra of D^*

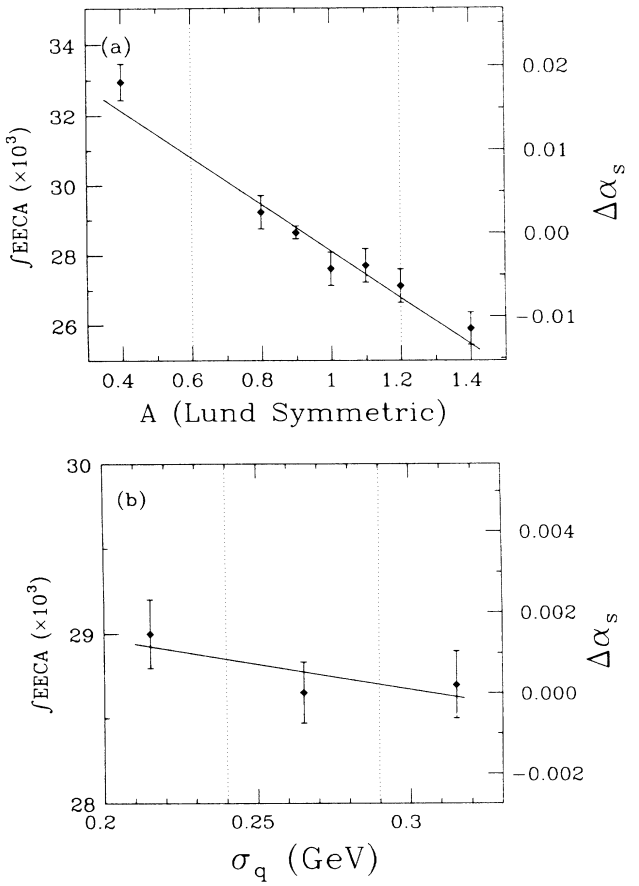

FIG. 8. Sensitivity of the EECA to model parameters. We show the integrated EECA from Monte Carlo samples at the generator level. The EECA is integrated over the range $28.8° < \chi < 90°$ and plotted vs (a) the parameter A in the Lund-symmetric fragmentation function, and (b) σ_q. The 1σ limits of these parameters are indicated with the dotted lines. The right-hand scales show the changes in the measured value of α_s which result from different choices of the parameter values.

mesons provide strong limits on the fragmentation function parameter ϵ_c (Ref. 37), and the fractional uncertainty on α_s introduced by the allowed variations is less than 1%.

The contributions from τ-pair and two-photon backgrounds are estimated with Monte Carlo simulations. They are found to have negligible effects on the α_s measurement.

It has been shown recently that the second-order QCD matrix elements underestimate the ratio of four- to three-jet events.[38] The deficiency in the four-jet rate presumably results from the lack of higher-order contributions. Thus we can roughly estimate the size of higher-order effects by artificially increasing the hard four-parton cross section accordingly. We carry out this procedure by doubling the four-parton rate[39] in the Monte Carlo simulations and then determining α_s. This results in a decrease of 0.005 in the measured value of α_s. We do not include this effect in our systematic errors,

TABLE III. Systematic errors on α_s measurement.

Source	PEP-5 EECA	Upgrade EECA
Data correction	3.3%	1.8%
σ_q	1.3%	1.1%
Fragmentation parameters	4.6%	4.6%

however, because we are quoting α_s at $O(\alpha_s^2)$.

The sources and their estimated contribution to the uncertainty in α_s are summarized in Table III. The data correction errors are derived from the uncertainties on C_1. The total systematic errors (combined in quadrature) are 0.009 (0.008) for PEP-5 (upgrade). We have not included the effects of different fragmentation models in the systematic errors; these are discussed separately in Sec. VI. We quote errors for the Lund model alone because it is the only $O(\alpha_s^2)$ model that adequately describes our data.

The results from the two configurations are now combined to give $\alpha_s(29\ \text{GeV}) = 0.158 \pm 0.003 \pm 0.008$. This α_s value is used to generate Monte Carlo events which are compared with the data in Figs. 9 and 10. The agreement is very good for both the EEC and the EECA. The data in these figures are fully corrected and are identical to the Mark II data shown in Fig. 5 except that the self-correlation contributions are removed from the lowest bin for clarity.

The QCD scale parameter Λ is related to α_s by

$$\alpha_s = \frac{2\pi}{\frac{33-2N_f}{6}\ln\left[\frac{Q^2}{\Lambda^2}\right] + \frac{153-19N_f}{33-2N_f}\ln\left[\ln\left[\frac{Q^2}{\Lambda^2}\right]\right]}, \tag{8}$$

in the modified minimal-subtraction ($\overline{\text{MS}}$) renormalization scheme,[40] where N_f is the number of flavors open.

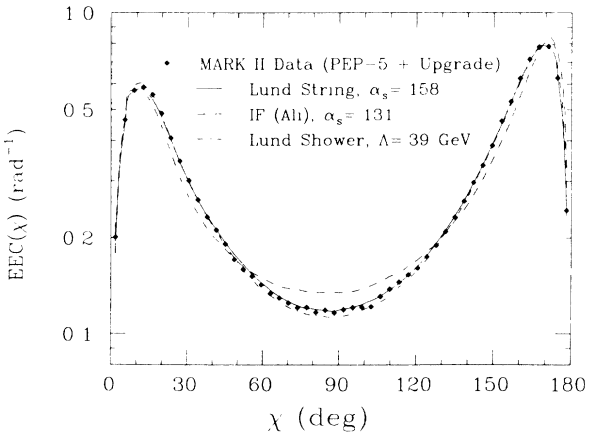

FIG. 9. Comparisons of EEC with Monte Carlo simulations. The predictions of several models are compared to the corrected EEC. The self-correlation contributions are removed from the lowest bin to make the figure more clear. The values of α_s or Λ_{LLA} are chosen from fits of the Monte Carlos to the EECA. The curve for IF (Hoyer) $\alpha_s = 0.102$ is not drawn because it coincides with the Ali curve.

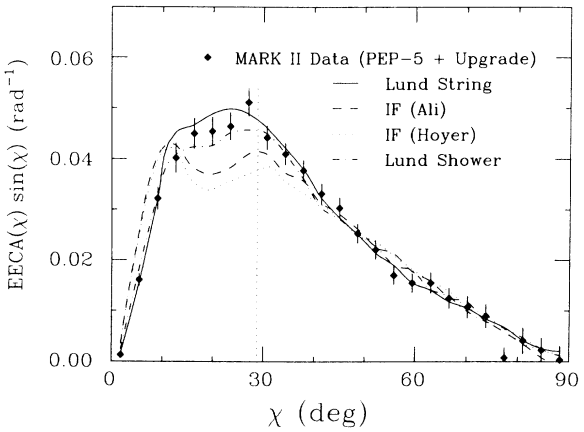

FIG. 10. Comparisons of EECA with Monte Carlo simulations. The results of the best fits to the EECA are shown for four different Monte Carlo generators: $\alpha_s=0.158$ for Lund string, $\alpha_s=0.131$ for Ali, $\alpha_s=0.102$ for Hoyer, and $\Lambda_{\rm LLA}=390$ MeV for Lund shower. The fits are performed over the region above the dotted line.

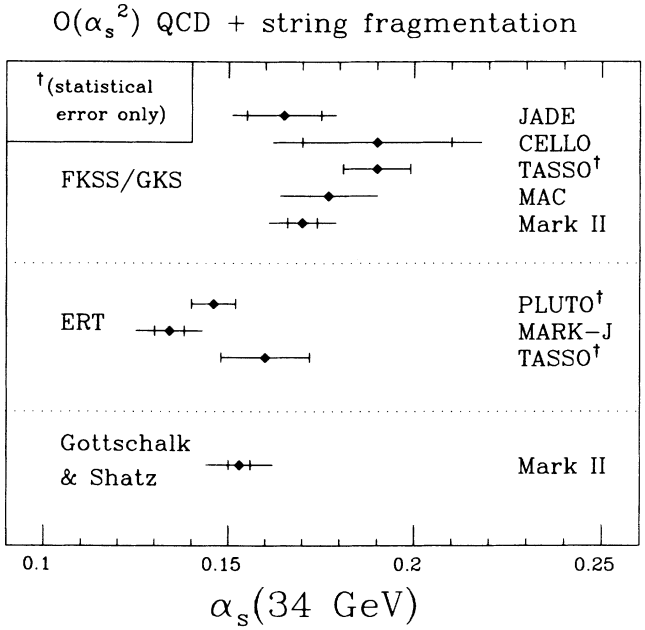

FIG. 11. Comparison of α_s measurements. Our value of α_s is compared to those from similar experiments, taken from Ref. 41. The horizontal bars represent the statistical and systematic errors (where available) added in quadrature. The vertical bars indicate the size of the statistical errors alone. All values were obtained by comparing the EECA with an $O(\alpha_s^2)$ matrix element plus Lund string fragmentation. The results are grouped according to the matrix element calculations used, which are indicated at the left. All measurements are at $\sqrt{s}=34$ GeV or rescaled to that value. The Mark II and MAC results are rescaled from 29 to 34 GeV according to Eq. (8) ($\Delta\alpha_s\approx-0.005$). The Mark J value is derived from their fit to Λ over the energy range 14–46.78 GeV. Where two points appear for the same experiment, they are not statistically independent.

At $Q=29$ GeV with $N_f=5$, our α_s value corresponds to $\Lambda_{\overline{\rm MS}}=330\pm40\pm70$ MeV.

Our result is compared with other EECA measurements[41] of α_s in Fig. 11. The present measurement is, as expected, in better agreement with the ERT values than with those obtained from the FKSS/GKS matrix element.[26] For the sake of comparison, we repeat our analysis using the GKS matrix element, and we obtain $\alpha_s(29\ {\rm GeV})=0.174\pm0.004\pm0.009$. Both results appear in the figure, where they are scaled to $Q=34$ GeV according to Eq. (8).

VI. MODEL COMPARISONS

Several alternatives exist to the string-fragmentation model which enjoy varying degrees of success in describing hadronic events at these energies. We examine some of these briefly in regard to the EEC and EECA.

Independent-fragmentation (IF) models are the most common alternative to string fragmentation. Since IF models do not automatically conserve momentum and energy, a particular method must be chosen to accomplish this, and this appears to be the dominant source of uncertainty in measuring α_s. The two cases we examine here are the Ali scheme,[42] where jet angles are adjusted and energies are preserved, and the Hoyer scheme,[27] where the opposite prescription is imposed. A fit to the EECA using the Ali scheme gives an α_s value of 0.131 ± 0.003 (statistical). Concurrent agreement with the EEC, however, cannot be achieved with any reasonable value of σ_q. The Hoyer scheme represents an even more extreme departure from the string model. It yields $\alpha_s=0.102\pm0.003$ (statistical) and similar disagreement with the EEC. The results of a best fit to the EECA are shown in Figs. 9 and 10. In each case, the model parameters A, B, and σ_q are tuned to give agreement with the average multiplicity and $p_\perp^{\rm out}$ from the data. These results concur with other experiments[3–8] which found that IF models tend to give lower values of α_s.

Finally, we compare our data with a leading-log QCD shower Monte Carlo simulation. As an example, we show the EEC from the Lund shower model, version 6.3 (Ref. 23). This model includes a matrix-element weighting of the first branching, and coherence effects are included by angular ordering of subsequent parton emission. As for the string model, the parameters have been adjusted to reproduce a variety of distributions.[28] The agreement of this model with the EEC and EECA data is quite good, as shown in Figs. 9 and 10.

In the shower model, the amount of gluon emission is determined by the QCD scale parameter $\Lambda_{\rm LLA}$. We determine this parameter from the EECA just as we measure α_s. We find $\Lambda_{\rm LLA}=390\pm30$ MeV (statistical). The definitions of $\Lambda_{\overline{\rm MS}}$ and $\Lambda_{\rm LLA}$ are sufficiently different that the agreement should be viewed as fortuitous.

The best agreement between the global features of the data and the shower model is obtained at a very low shower cutoff value ($Q_0=1$ GeV) (Ref. 28). The EECA,

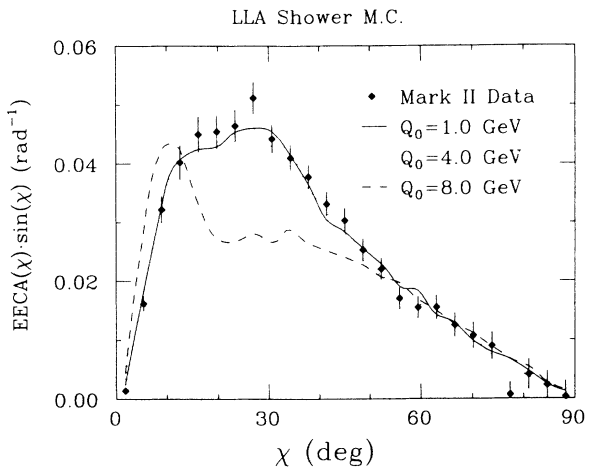

FIG. 12. Cutoff sensitivity in the shower model. The EECA predicted by the Lund shower Monte Carlo simulation is shown for three different values of the shower cutoff mass, Q_0. The fragmentation parameters A, B, and σ_q are adjusted for each Q_0 value to maintain a constant multiplicity and p_1^{out} spectrum, but Λ_{LLA} is fixed at 400 MeV.

however, shows little sensitivity to this cutoff for $Q_0 \lesssim 4$ GeV, as shown in Fig. 12. In contrast with the results of PLUTO (Ref. 8), who showed that an earlier shower model was unable to describe their EECA, this good agreement reflects recent improvements in leading-log models.

VII. SUMMARY

We have studied the energy-energy correlation in e^+e^- annihilation into hadrons at 29 GeV. We have used data from the Mark II detector both before and after its upgrade for the SLC, and we find good agreement between the two data sets. We also compare our data to the published results of other experiments. We find reasonable agreement with the EEC and EECA distribution from the MAC detector at SLAC, which has also operated at 29 GeV. This agreement is best in the perturbative region of the EECA ($\chi \gtrsim 30°$). PETRA experiments at 34 GeV also compare well in this region.

We determine α_s from our EECA measurement. The results from the PEP-5 and upgrade data agree well, and give a combined value of $\alpha_s = 0.158 \pm 0.003 \pm 0.008$ when we use the matrix-element calculation of Gottschalk and Shatz and string fragmentation. This result is in reasonable agreement with similar measurements made with the ERT matrix elements, and is about 10% lower than FKSS/GKS determinations. Independent fragmentation models yield considerably lower values of α_s (0.11–0.14).

Both the EECA and EEC are described well by the Lund string model, but cannot be simultaneously fit with independent-fragmentation models. The recent Lund leading-log shower model also describes both distributions well with a QCD scale parameter of $\Lambda_{\text{LLA}} = 390 \pm 30$ MeV.

ACKNOWLEDGMENTS

The authors are grateful to S. Bethke for many useful discussions and for providing computer code for the Gottschalk and Shatz matrix element. This work was supported in part by Department of Energy Contracts Nos. DE-AC03-81ER40050 (CIT), DE-AA03-76SF00010 (UCSC), DE-AC02-86ER40253 (Colorado), DE-AC02-76ER03064 (Harvard), DE-AC03-83ER40103 (Hawaii), DE-AC02-84ER40125 (Indiana), DE-AC03-76SF00098 (LBL), DE-AC02-84ER40125 (Michigan), and DE-AC03-76SF00515 (SLAC), and by the National Science Foundation (Johns Hopkins).

[a]Present address: Universidad Autónoma de Barcelona, Bellaterra, Spain.
[b]Present address: University of Chicago, Chicago, IL 60637.
[c]Present address: Harvard University, Cambridge, MA 02138.
[d]Present address: University of Pennsylvania, Philadelphia, PA 19104.
[e]Present address: Therma-Wave Corporation, Fremont, CA 94539.
[f]Present address: University of California, Berkeley, CA 94720.
[g]Present address: Brookhaven National Laboratory, Upton, NY 11973.
[h]Present address: Vista Research Inc., 3600 Bayshore Road, Palo Alto, CA 94303.
[i]Present address: CERN, CH-1211, Genève 23, Switzerland.
[j]Present address: Laboratory für Hochenergie Physik Bern, CH-3012 Bern, Switzerland.
[k]Present address: Columbia University, New York, 10027.
[l]Present address: Université de Genève, CH-1211, Genève 4 Switzerland.
[m]Present address: University of Illinois, Urbana, IL 61801.
[n]Present address: University Pierre Marie Curie, F-75230, Paris, France.
[o]Present address: Oxford University, Oxford, England.

[1]C. L. Basham *et al.*, Phys. Rev. D **17**, 2298 (1978).
[2]H.-J. Behrend *et al.*, Z. Phys. C **14**, 95 (1982).
[3]H.-J. Behrend *et al.*, Phys. Lett. **138B**, 31 (1984).
[4]W. Bartel *et al.*, Z. Phys. C **25**, 231 (1984).
[5]M. Althoff *et al.*, Z. Phys. C **26**, 157 (1984).
[6]E. Fernandez *et al.*, Phys. Rev. D **31**, 2724 (1985).
[7]B. Adeva *et al.*, Phys. Rev. Lett. **50**, 2051 (1983); B. Adeva *et al.*, *ibid.* **54**, 1750 (1985).
[8]Ch. Berger *et al.*, Z. Phys. C **28**, 365 (1985).
[9]S. D. Ellis, Phys. Lett. **117B**, 333 (1982).
[10]A. Ali and F. Barreiro, Phys. Lett. **118B**, 155 (1982).
[11]T. Sjöstrand, Z. Phys. C **26**, 93 (1984).
[12]D. Schlatter *et al.*, Phys. Rev. Lett. **49**, 521 (1982).
[13]R. H. Schindler *et al.*, Phys. Rev. D **24**, 78 (1981).
[14]Proposal for the Mark II at SLC, Report No. CALT-68-1015, 1983 (unpublished).

[15]G. Hanson, Nucl. Instrum. Methods **A252**, 343 (1986).
[16]W. T. Ford *et al.*, Nucl. Instrum. Methods **A255**, 480 (1987).
[17]R. C. Jared *et al.*, I.E.E.E. Trans. Nucl. Sci. **N-S33**, 916 (1986).
[18]J. D. Bjorken and S. J. Brodsky, Phys. Rev. D **1**, 1416 (1970); G. Hanson *et al.*, Phys. Rev. Lett. **35**, 1609 (1975); we used the definition from C. Berger *et al.*, Phys. Lett. **82B**, 449 (1979).
[19]Our choice of bin intervals follows a convention established by CELLO (Ref. 2) and followed by JADE (Ref. 4) and MAC (Ref. 6). For more details and comparisons with other experiments see D. R. Wood, Ph.D. thesis, 1986, Report No. LBL-24208.
[20]M. Chen and L. Garrido, Phys. Lett. B **180**, 409 (1986).
[21]F. A. Berends and R. Kleiss, Nucl. Phys. **B178**, 141 (1981).
[22]P. C. Rowson *et al.*, Phys. Rev. Lett. **54**, 2580 (1985).
[23]T. Sjöstrand, Comput. Phys. Commun. **39**, 347 (1986); T. Sjöstrand, M. Bengtsson, Report No. LU TP 86-22, 1986 (unpublished).
[24]This is an improved version with baryon production based on A. Ali *et al.*, Phys. Lett. **93B**, 155 (1980).
[25]H. M. Schellman, Ph.D. thesis, 1984, Report No. LBL-18699.
[26]T. D. Gottschalk and M. P. Shatz, Phys. Lett. **B150**, 451 (1985); Report No. Calt-68-1172,-1173, 1985 (unpublished); T. D. Gottschalk (private communication). It was pointed out by M. Chen [in *How far are we from Gauge Forces,* proceedings of the International School of Subnuclear Physics "Ettore Majorana," Erice, Italy, 1983, edited by A. Zichichi (Plenum, New York, 1983), Vol. 21, p. 624] that the FKSS method yields a 20% higher α_s value than that obtained by the ERT method.
[27]P. Hoyer *et al.*, Nucl. Phys. **B161**, 349 (1979). We implement the Hoyer scheme with the Lund symmetric fragmentation function with parameters $A=1.1$, $B=0.7$, $\sigma_q=0.295$ GeV.
[28]A. Petersen *et al.*, Phys. Rev. D **37**, 1 (1988).
[29]These integrals are shown for several experiments and models in Ref. 28.
[30]R. K. Ellis, D. A. Ross, and A. E. Terrano, Nucl. Phys. **B178**, 421 (1981).
[31]F. Gutbrod, G. Schierholz, and G. Kramer, Z. Phys. C **21**, 235 (1984); K. Frabricius, G. Kramer, G. Schierholz, and I. Schmitt, Phys. Lett. **97B**, 43 (1980).
[32]H. Aihara *et al.*, Z. Phys. C **28**, 31 (1985).
[33]M. Althoff *et al.*, Z. Phys. C **29**, 29 (1985); H. Aihara *et al.*, Phys. Rev. Lett. **57**, 945 (1986); P. D. Sheldon *et al.*, *ibid.* **57**, 1398 (1986).
[34]The parameters used for the Lund string model are $y_{\min}=0.015$, $A=0.9$, $B=0.7$, and $\sigma_q=0.265$ GeV/c. Parameters for the Lund shower model are $Q_0=1.0$ GeV, $A=0.45$, $B=0.9$, and $\sigma_q=0.230$ GeV/c.
[35]B. Andersson *et al.*, Phys. Rep. **97**, 31 (1983).
[36]C. Peterson *et al.*, Phys. Rev. D **27**, 105 (1983).
[37]S. Bethke, Z. Phys. C **29**, 175 (1985).
[38]W. Bartel *et al.*, Z. Phys. C **33**, 23 (1986).
[39]In this case, we define the individual n-parton rates by a $y_{\min}$ cut of 0.04.
[40]M. Dine and S. Sapirstein, Phys. Rev. Lett. **43**, 668 (1979); W. Marciano, Phys. Rev. D **29**, 580 (1984).
[41]B. Naroska, Phys. Rep. **148**, 67 (1987), and references therein.
[42]A. Ali *et al.*, Phys. Lett. **93B**, 155 (1980). We implement the Ali scheme with the Lund symmetric fragmentation function with parameters $A=0.75$, $B=0.7$, $\sigma_q=0.285$ GeV.